e-ISSN 2757-5195

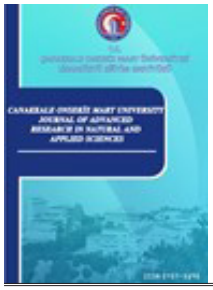

Çanakkale Onsekiz Mart University
Journal of Advanced Research in Natural and Applied Sciences
Open Access

doi.org/10.28979/jarnas.1003367 2022, Cilt 8, Sayı 1, Sayfa: 63-75 dergipark.org.tr/tr/pub/jarnas

Calculation Of Gruneisen Parameter, Compressibility, And Bulk Modulus as Functions Of Pressure In $(C_6H_5CH_2NH_3)_2PBI_4$

Arzu KURT[1]*

[1]Department of Energy Management, Faculty of Applied Sciences, Canakkale Onsekiz Mart University, Canakkale, Turkey

Article History

Received: 01.10.2021
Accepted: 03.11.2021
Published: 10.03.2022

Research Article

Abstract − Hybrid organic-inorganic perovskites (HOIPs) exhibit multiple structural phase transitions, which result in enhanced mechanical and electronic properties of these perovskites. Order-disorder of organic components was thought to be the main factor to cause these phase transitions up to the last decade; however, recent research about HOIPs have shown that the structural phase transition also occurs with the induced pressure or temperature. The research studies related to the pressure have attracted a great deal of scholarly interest due to its contribution to the func-tionality of HOIPs in many current applications. Two-dimensional halide perovskites having been synthesized in the last few years have been increasingly studied thanks to its superior hysteresis in flexibility and mechanical properties under pressure. It is important to understand and model theoretically how induced pressure affects mechanical and electronic properties of (PMA)2PbI4 in order to develop new potential applications in optoelectron-ics. In this study, the isothermal mode-Grüneisen parameter, the isothermal compressibility, and the bulk modulus were calculated as functions of pressure at ambient temperature by using the calculated Raman frequencies and observed volume data for the selected IR modes in (PMA)2PbI4. These calculated parameters were compared with the observed measurements reported for the Pbca, Pccn and Pccn (isostructural) phases in the studied perovskites. The results obtained in the present study, which were highly compatible with the experimental measurements, showed that (PMA)2PbI4 is usable in optoelectronic applications

Keywords − *HOIPs, Phase Transition, Grüneisen Parameter, Bulk Modulus.*

1. Introduction

Hybrid Organic-Inorganic Perovskites (HOIPs) have been attracting a considerable amount of scientific attention due to their potential for photovoltaic, optoelectronic, and electronic applications in the last quarter. Power conversion efficiency in photovoltaics can be increased up to 24.2% by using HOIPs as active materials in photovoltaic (PV) productions processes. Therefore, a great many scientists have intended to research mechanical and electronic properties of HOIPs over the last decades (Kooijman, Muscarella, & Williams, 2019). Perovskites whose general formula is ABX_3 is a member of HOIPs (Breternitz & Schorr, 2018). This type of HOIPs has a well-defined multiple quantum well, which can be altered by optimizing the organic-inorganic layers (Kawano et al., 2014). Thanks to these properties, HOIPs make a great material for photovoltaic applications, light-emitting diode, and light detectors (Bandiello et al., 2016; Fang et al., 2015; Khadka, Shirai, Yanagida, Ryan, & Miyano, 2017; Qin, Dong, & Hu, 2015). Recently, 2D (two dimensional) HOIPs are reported to have excellent stability under ambient conditions (Dou et al.,2015; Yang et al., 2017). $(C_6H_5CH_2NH_3)_2PbI_4$ (shortly; $(PMA)_2PbI_4$) is a good example of 2-D HOIPs, which exhibit multiple phase transitions under pressure at ambient temperature. Tian et al. have carried out X-ray diffraction (XRD) experiments to investigate the crystal structure in $(PMA)_2PbI_4$ and the change of optical properties at various pressures. They have obtained that all the Bragg diffraction peaks yield slightly high values with the increasing pressure as expected, while they report an additional peak at 4.6 GPa and

[1] arzukurt@comu.edu.tr
*Sorumlu Yazar / Corresponding Author

splitting peak at 7.7 GPa. They have attributed these anomalies to a possible phase transition (Tian et al., 2020). These pressure-induced phase transitions are associated with Pbca to Pccn at 4.6 GPa and Pccn to Pccn (isostructural) at 7.7 GPa. Although there is no explicit emerging peak in the XRD pattern at 7.7 GPa in the research by Tian et al (2020), the literature incorporates works reporting by considering the splitting of peak in XRD pattern that similar HOIPs exhibit isostructural phase transitions (Wang, Wang, Xiao, Zeng, & Zou, 2016). Apart from the operationalization of pressure as a good tool to provide more effective properties by lattice contraction without the involvement of composition change, there are various other efforts, e.g., chemically manipulating dimensionality and introducing additional properties into HOIPs, (Mao, Chen, Ding, Li, &Wang, 2018; Ren et al.,2020). The first study about pressure induced transition was carried on $CH_3NH_3PbBr_3$ perovskite by Wang et al. in 2015 (Y. Wang et al., 2015). After this work, the amount of research related to the behaviors of HOIPs under pressure has substantially increased, and thus many structures of HOIPs have been discovered, which are applicable in PV, photoluminescence (PL), and optoelectronics (Ou et al., 2019; Ou et al., 2018; Ren et al., 2019; L. Wang et al., 2017; Yuan et al., 2019). The main goal of the studies on administering high pressure on HOIPs has been to adjust the band gap with the recovery of metastable phase in industrial applications. Although many experimental studies have been carried out to explain adequately the pressure dependency of mechanical and electronic properties of HOIPs, there has been a need for a theoretical approach to account for these macroscopic thermodynamic parameters without making expensive and grueling experiment.

In this study, I calculated the pressure dependency of the Grüneisen parameter (γ_T), compressibility (κ_T) and the bulk modulus (β) values of $(PMA)_2PbI_4$ for 794 cm^{-1} ν_s(C-N), 931 cm^{-1}, 970 cm^{-1} and 1045 cm^{-1} β (C-H), 1212 cm^{-1} δ(C-H), 1496 cm^{-1} $\delta(NH_3^+)$, 2903 cm^{-1} $\nu_s(CH_2^+)$, and 3068 cm^{-1} $\nu_s(NH_3^+)$ modes at ambient temperature by using the experimental volume data and Raman frequencies. Besides, the IR wavenumbers of $(PMA)_2PbI_4$ were calculated for 794 cm^{-1} ν_s(C-N), 931 cm^{-1}, 970 cm^{-1} and 1045 cm^{-1} β (C-H), 1212 cm^{-1} δ(C-H), 1496 cm^{-1} $\delta(NH_3^+)$, 2903 cm^{-1} $\nu_s(CH_2^+)$, and 3068 cm^{-1} $\nu_s(NH_3^+)$ modes in $(PMA)_2PbI_4$ through the calculated Grüneisen parameters of these IR modes and experimental volume data in the literature (Tian et al., 2020). Moreover, the calculated bulk modulus was discussed in consideration of the available literature for all the IR modes in $(PMA)_2PbI_4$.

2. Materials and Methods

The Grüneisen parameter, slightly altered with the volume of a crystal lattice as a function of pressure and/or temperature is dimensionless. Changed temperature and/or pressure affect the size or dynamics of a crystal lattice; thus, familiar macroscopic thermodynamic properties, such as heat capacity and thermal expansion, tend to change, leading to slight shifts in the vibrational frequencies of atoms in a molecular crystal. It is almost impossible to determine the Grüneisen parameter experimentally. Because of that, investigating macroscopic parameters necessitates a detailed knowledge of the phonon distribution spectrum of the material, while researching microscopic parameters entails experimental measurements of the thermodynamic properties at high pressure and temperature. This duality can be resolved by associating the Grüneisen parameter with the vibrational frequency of the atom in the molecular crystal. In 1912, Grünesien indicated in his original article that the Grüneisen parameter (denoted by γ) is related to the volume dependence of mode frequency by regarding the quantum harmonic oscillator of Einstein's theory as a mode of crystal vibration (Grüneisen, 1912)(Grüneisen, 1912)(Grüneisen, 1912);

$$\gamma = \alpha K_T / \rho C_V \tag{2.1}$$

α, K_T, ρ, and C_V are volume expansion coefficient, isothermal bulk modulus, density, and specific heat at constant volume, respectively. Despite quantum mechanics begin with Planck's theory of blackbody radiation in 1900, Boltzmann's identification about the quantization of thermally excited atomic energy level and transition between these levels was a crucial for definition of transition probabilities between these levels. The relation between the quantized energy of radiation and its frequency is explained by Planck's theory (Planck, 1901);

$$\Delta E = h\nu \tag{2.2}$$

where h is Planck constant and ν is the frequency of photon. Planck's theory explains the spectral density of electromagnetic radiation emitted by a black body in thermal equilibrium at a constant temperature T. Planck's theory is valid for not only the radiation but also the energies of oscillatory phenomena at the atomic energy level. The probability of transition between two atomic states (from 1st to 2nd state) in a molecule or an atom driven by temperature is referred to as the Boltzmann factor, which is characterized only by these two states' energy difference:

$$\frac{p_2}{p_1} = e^{-\frac{\Delta E}{kT}} \tag{2.3}$$

where $\Delta E=E_2-E_1$, k is the Boltzman constant and T is ambient temperature. In generally, the probability of transition from the nth state relative to the ground state ($n=0$) can be defined by integrating the Planck's formula into the Boltzmann factor;

$$p(n) = p(0)e^{-\frac{nh\nu}{kT}} \tag{2.4}$$

where $p(n)$ is the probability of occupation of state n, $p(0)$ is the probability of occupation of ground state, n is the state of atom. If the nth state in an atom is filled with electrons, the energy of the state ($nh\nu$) is added to the total energy of atom by multiplying the probability of the state energy;

$$\Delta E(n) = nh\nu p(n) = p(0)nh\nu e^{(-nh\nu/kT)} \tag{2.5}$$

Adding the contributions by all the states, the average total energy in an atom can be defined as;

$$E = \sum_{n=0}^{\infty} E(n) = \frac{h\nu}{[\exp(h\nu/kT) - 1]} \tag{2.6}$$

This energy corresponds to the thermal energy of a single mode in crystal oscillation with a natural frequency ν, which is function of volume, as in Einstein's theory (Einstein, 1907). The Einstein model, represented by Eq. (2.6), is the starting point for Grüneisen's theory (Stacey & Hodgkinson, 2019). Each mode of the frequency ν_i in the crystal has its own Grüneisen parameter value;

$$\gamma_i = -\left(\frac{\partial ln\nu_i}{\partial lnV}\right)_T \tag{2.7}$$

where ν_i is the frequency of the ith mode, and V is the volume (Stacey & Hodgkinson, 2019). Differentiating Eq. (2.7) with respect to pressure (P), the isothermal Grüneisen parameter is reduced as;

$$\gamma_{T,i} = -\frac{V}{\nu}\frac{(\partial\nu_i/\partial P)_T}{(\partial V/\partial P)_T} \tag{2.8}$$

the frequency (ν) and the volume (V) in Eq.(2.8) are dependent only on pressure (P) and T is ambient temperature and constant. The experimental volume data of $(PMA)_2PbI_4$ show a parabolic change with pressure (Tian et al., 2020), so it was assumed that the function of the crystal volume is a second-order polynomial function of pressure as reported in my previous study (Kurt, 2020);

$$V_T(P) = a_o + a_1 P + a_2 P^2 \tag{2.9}$$

a_o, a_1 *and* a_2 are the constants under isothermal condition. In order to determine these constants, Eq. (2.9) was fitted to the experimental data in the literature (Tian et al., 2020) for the orthorhombic Pbca (0<P<4.6 GPa), orthorhombic Pccn (4.6<P<7.7 GPa) and orthorhombic Pccn(isostructural) (7.7<P<20 GPa) phases, as shown in Fig. 1 and given in Table 1. The frequencies of the IR modes in $(PMA)_2PbI_4$ were also expressed as the second-order polynomial function with pressure, like volume data, and the relation of the frequencies was assumed as a function of pressure,

$$\nu_T(P) = b_o + b_1 P + b_2 P^2 \tag{2.10}$$

b_0, b_1 and b_2 are the constant coefficients for each mode. The coefficients were determined by fitting Eq. (2.10) to the experimental data (Tian et al., 2020) for ν_s(C-N), β(C-H), δ(C-H), δ(NH_3^+), ν_s(CH_2^+), and ν_s(NH_3^+) IR modes for each phase in $(PMA)_2PbI_4$, as presented in Table 2. Then, by using the calculated volume data through the obtained coefficient from the experimental volume data, the isothermal Grüneisen parameter as a function of pressure was determined for 794 cm^{-1} ν_s(C-N), 970 cm^{-1} β (C-H), 1212 cm^{-1} δ(C-H), and 2903 cm^{-1} ν_s(CH_2^+) IR modes (Fig. 2).

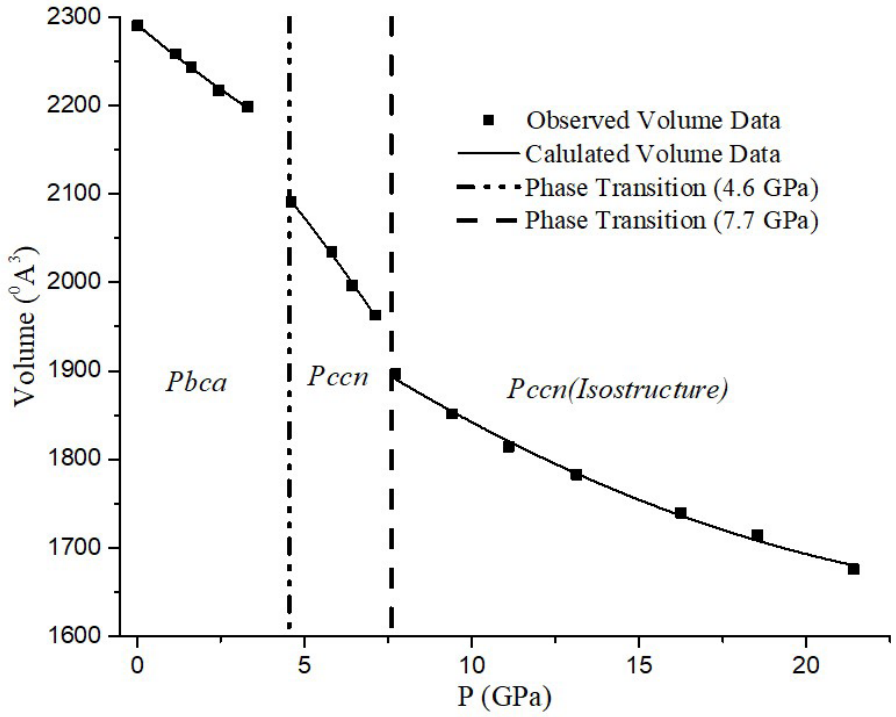

Figure 1. Observed and calculated volume data for Pbca, Pccn, and Pccn(isostructural) phases.

Table 1

a_0, a_1, and a_2 values from Eq. (2.9) for Pbca, Pccn, and Pccn (isostructural) phases of $(PMA)_2PbI_4$ at room temperature.

$(PMA)_2PbI_4$	a_0 $(A^0)^3$	$-a_1$ $((A^0)^3/ GPa)$	a_2 $((A^0)^3/ GPa^2)$	$V_0(A^o)^3$
Pbca	2291.61	31.79	0.98	2291.61
Pccn	2271.55	30.68	-1.81	2271.55
Pccn(Isostruc.)	2085.83	28.95	0.46	2085.83

By integrating Eq. (2.7), the frequency value as a function of pressure for each mode can be calculated as follows:

$$\nu_T(P) = \nu_0 exp[-\gamma_T \ln(V_T(P)/V_0)] + Const. \quad (2.11)$$

The vibrational frequencies of 794 cm^{-1} ν_s(C-N), 931 cm^{-1}, 970 cm^{-1} and 1045 cm^{-1} β (C-H), 1212 cm^{-1} δ(C-H), 1496 cm^{-1} $\delta(NH_3^+)$, 2903 cm^{-1} $\nu_s(CH_2^+)$, and 3068 cm^{-1} $\nu_s(NH_3^+)$ IR modes were calculated as functions of pressure by excluding the constant term for each phase through the indicated Grüneisen parameter (Eq. 2.8) and the volume value (Eq. 2.9). The calculations for the vibrational frequencies of each IR mode did not, however, correspond to the observed frequencies. Hence, Eq. (2.11) had to be corrected with a pressure-dependent second-order polynomial, which is a constant term. In order to calculate exactly the IR frequencies of ν_s(C-N), β(C-H), δ(C-H), $\delta(NH_3^+)$, $\nu_s(CH_2^+)$, and $\nu_s(NH_3^+)$ modes, the constants of the additional pressure-dependent polynomial had to be determined.

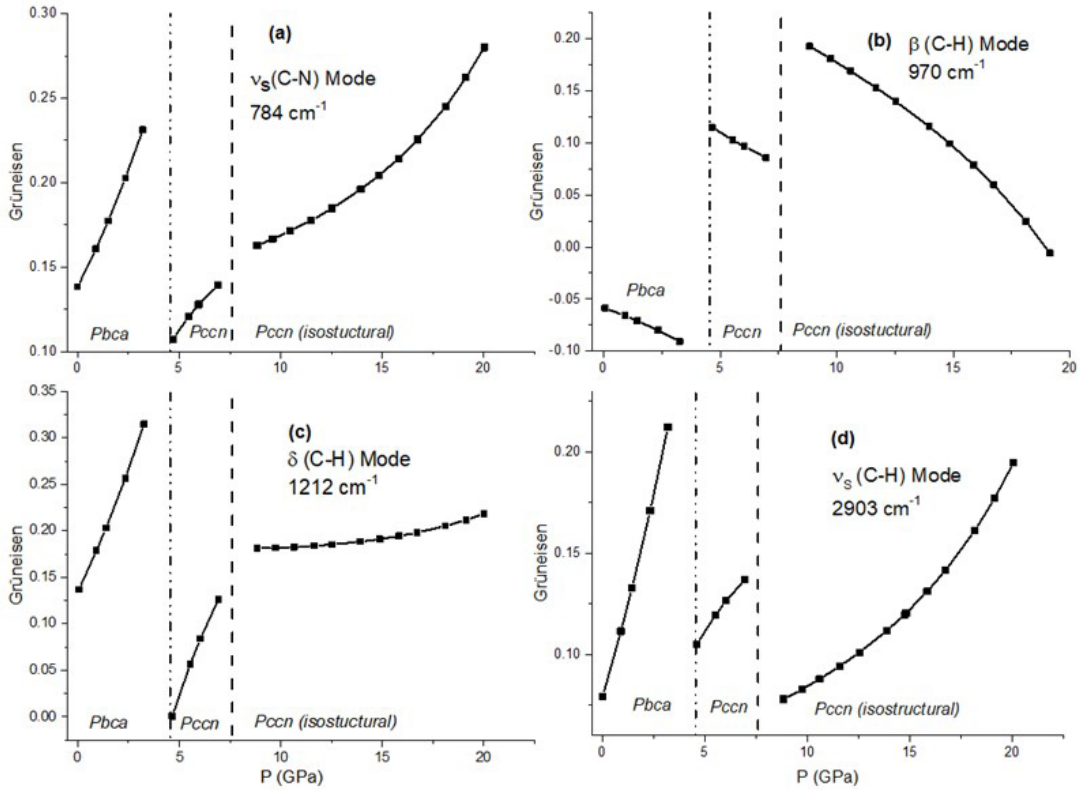

Figure 2. Grüneisen parameter of isothermal mode (Eq. 2.8) vs. pressure for Pbca, Pccn, and Pccn(isostructural) phases.

c_0, c_1, and c_2 are the constants of the additional polynomial. The coefficients were determined by iterating Eq. (2.12) to the experimental frequencies data at room temperature (Tian et al., 2020) (Table 3). Hence, the predicted IR frequencies of the ν_s(C-N), β(C-H), δ(C-H), δ(NH_3^+), ν_s(CH_2^+), and ν_s(NH_3^+) modes with the observed data as functions of pressure for $(PMA)_2PbI_4$ were plotted in Fig. 3, 4, and 5.

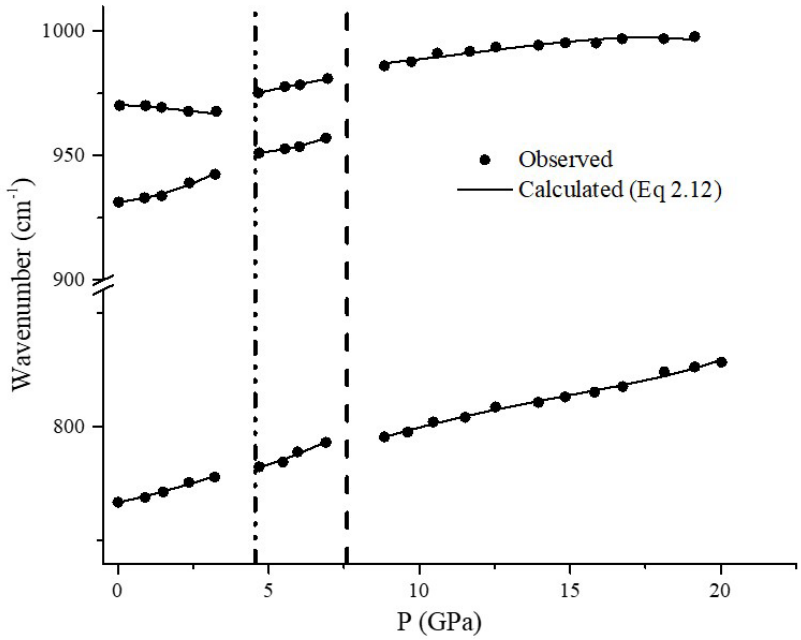

Figure 3. IR wavenumbers of 794 cm^{-1} ν_s(C-N), 931 cm^{-1}, 970 cm^{-1}, β (C-H), modes as function of pressure for Pbca, Pccn, and Pccn(isostructural) phases.

$$\nu_T(P) = c_0 + c_1P + c_2P^2 + \nu_0 exp[-\gamma_T \ln(V_T(P)/V_0)] \quad (2.12)$$

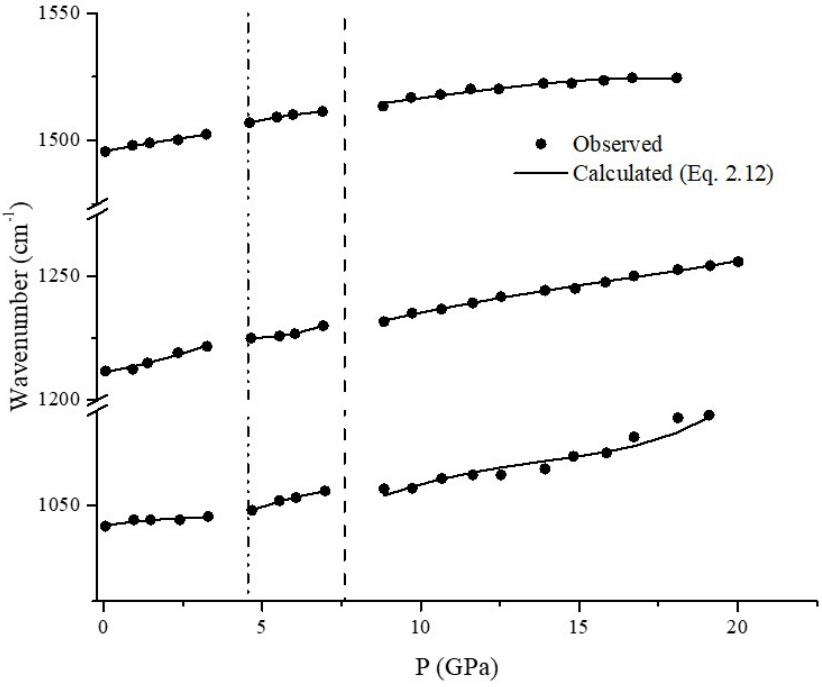

Figure 4. IR wavenumbers of 1045 cm^{-1} β (C-H), 1212 cm^{-1} δ(C-H), 1496 cm^{-1} δ(NH_3^+)modes as function of pressure for Pbca, Pccn, and Pccn(isostructural) phases.

Bulk modulus is a constant used to describe the elasticity of a solid under pressure. In other words, this constant is a measure of a substance's capability of resisting volumic changes under high pressure and sometimes named as incompressibility. If a material has a high bulk modulus constant, the reduced volume under high pressure grows back to its initial volume when the pressure is removed. Bulk modulus is derived from compressibility and inverse of this parameter. In this study, the pressure-dependent isothermal compressibility and bulk modulus $(PMA)_2PbI_4$ were determined for the Pbca, Pccn and Pccn(isostructural) phases as well. In thermodynamics, the isothermal compressibility is calculated by the following relation;

$$\kappa_T = -\frac{1}{V}\left(\frac{\partial V}{\partial P}\right)_T \tag{2.13}$$

By inserting Eq. (2.8) and Eq. (2.12) in Eq.(2.13), the isothermal compressibility can be deduced as a function of IR wavenumber shift. In this way, one can calculate the isothermal compressibility through the Raman frequencies shift and the Grüneisen parameter by using the below relation;

$$\kappa_T = \frac{1}{\gamma_T}\frac{1}{\nu}\left(\frac{\partial \nu}{\partial P}\right)_T \tag{2.14}$$

Fig. 6 shows the calculated pressure dependence of the isothermal compressibility for all the phases. Additionally, the bulk modulus was determined for all the phases in $(PMA)_2PbI_4$ by making linear regression to the inverse of the calculated isothermal compressibility (Fig. 7). The slope and intercept of the linear regression of the calculated bulk modulus are shown in Fig. 7.

3. Results and Discussion

Pressure, potentially causing changes in interatomic distance and molecular bond length, can be used to control the mechanic and electronic properties of solids in thermodynamics. Shrinkage in length not only affect mechanical properties but also electronic structure in an atom or molecules. From the viewpoint of mechanical properties, high pressure may cause a conversion from weak van der Waals (π), and hydrogen bonds to strong covalent or ionic bonds, as a result of which the coordination number increases. In terms of electronic properties, one of the most remarkable effects of pressure is a fast increase in the kinetic energies of electrons than in their potential energies. As a result of these alterations, a general trend occurs toward electron delocalization, which leads to pressure-induced energy band expansion, gap closure, and metallization (Zhang, Wang, Lv, & Ma, 2017). The pressure-induced mechanical and electronic changes lead to small changes in macroscopic properties, such as compressibility and bulk modulus. It is possible to produce and develop new types of HOIP structures by advancing pressure under room temperature. Further, the phase transition mechanisms of HOIPs can be managed by controlling pressure. In this study, firstly Eq. (2.9) was fitted to the experimental volume data available in the literature (Fig. 1) (Tian et al., 2020), and then the coefficients of Eq. (2.9) were determined for all the phases in $(PMA)_2PbI_4$ (Table 1). Subsequently, the IR frequencies of 794 cm^{-1} ν_s(C-N), 931 cm^{-1}, 970 cm^{-1} and 1045 cm^{-1} β (C-H), 1212 cm^{-1} δ(C-H), 1496 cm^{-1} $\delta(NH_3^+)$, 2903 cm^{-1} $\nu_s(CH_2^+)$, and 3068 cm^{-1} $\nu_s(NH_3^+)$ modes were calculated as functions of pressure through the calculated volume and Grüneisen value for the ($(PMA)_2PbI_4$-I, Pbca), ($(PMA)_2PbI_4$-II, Pccn), and ($(PMA)_2PbI_4$-III, Pccn isostructural) phases at room temperature. Lastly, the compressibility and bulk modulus of the studied HOIPs were determined with Eq. (2.14) for all the phases.

Table 2

Values of the b_0, b_1, and b_2 from Eq. (2.10) for Pbca, Pccn, and Pccn(isostructural) phases of $(PMA)_2PbI_4$ at room temperature.

$(PMA)_2PbI_4$	**Pbca Phase**			
$\nu_T(P)$	**b_0 (cm^{-1})**	**b_1 (cm^{-1}/GPa)**	**b_2 (cm^{-1}/GPa^2)**	**ν_0 (cm^{-1})**
784(cm^{-1}) ν_s(C-N)	783.34	1.50	$9.61x10^{-2}$	783.34
931(cm^{-1}) β(C-H)	931.27	1.34	$6.97x10^{-1}$	931.27
970(cm^{-1}) β(C-H)	970.50	-0.78	$3.57\ x10^{-2}$	970.50
1045(cm^{-1})β(C-H)	1044.75	1.27	$-1.86\ x10^{-1}$	1044.75
1212(cm^{-1})δ(C-H)	1211.14	2.26	$3.36\ x10^{-1}$	1211.14
1496(cm^{-1})δ(NH_3^+)	1495.75	2.36	$-1.07\ x10^{-2}$	1495.75
2903(cm^{-1})ν_s(CH_2^+)	2903.89	-3.16	$-6.19\ x10^{-1}$	2903.89
3068(cm^{-1}) ν_s(NH_3^+)	3067.60	-1.49	$1.48\ x10^{-1}$	3067.60
	Pccn Phase			
784(cm^{-1}) ν_s(C-N)	787.85	$-5.58x10^{-1}$	$2.66\ x10^{-1}$	787.85
931(cm^{-1}) β(C-H)	962.47	-5.83	$7.32\ x10^{-1}$	962.47
970(cm^{-1}) β(C-H)	962.74	2.87	$3.44\ x10^{-2}$	962.74
1045(cm^{-1})β(C-H)	1027.61	6.13	$-3.41\ x10^{-1}$	1027.61
1212(cm^{-1})δ(C-H)	1245.60	-8.89	$9.58\ x10^{-1}$	1245.60
1496(cm^{-1})δ(NH_3^+)	1484.24	6.98	$-4.42\ x10^{-1}$	1484.24
2903(cm^{-1})ν_s(CH_2^+)	2877.58	1.49	$-8.99\ x10^{-1}$	2877.28
3068(cm^{-1}) ν_s(NH_3^+)	3062.40	$1.73\ x10^{-2}$	$-7.97\ x10^{-2}$	3062.40
	Pccn(Isostructure) Phase			
784(cm^{-1}) ν_s(C-N)	782.25	1.92	$-1.76\ x10^{-2}$	782.25
931(cm^{-1}) β(C-H)	-	-	-	-
970(cm^{-1}) β(C-H)	959.65	3.98	$-1.05\ x10^{-1}$	959.65
1045(cm^{-1})β(C-H)	1056.81	-1.28	$1.13\ x10^{-1}$	1056.81
1212(cm^{-1})δ(C-H)	1207.60	3.11	$-3.48\ x10^{-2}$	1207.60
1496(cm^{-1})δ(NH_3^+)	1486.22	4.22	$-1.16\ x10^{-1}$	1486.22
2903(cm^{-1})ν_s(CH_2^+)	2855.09	-1.72	$-4.19\ x10^{-2}$	2855.09
3068(cm^{-1}) ν_s(NH_3^+)	3055.68	0.51	$-6.54\ x10^{-2}$	3055.68

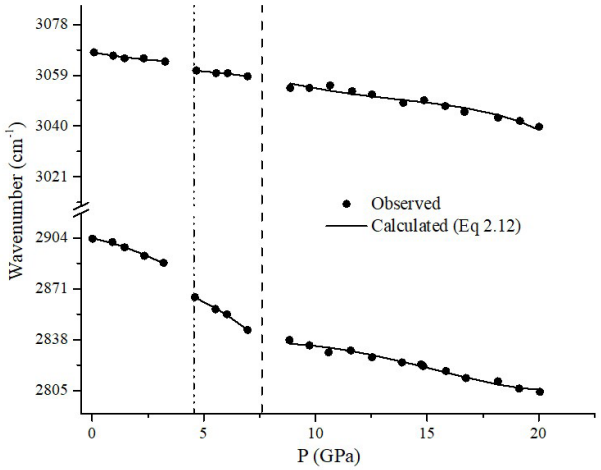

Figure 5. IR wavenumbers of 2903 cm^{-1} $\nu_s(CH_2^+)$, and 3068 cm^{-1} $\nu_s(NH_3^+)$ modes as function of pressure for Pbca, Pccn and Pccn(isostructural) phases.

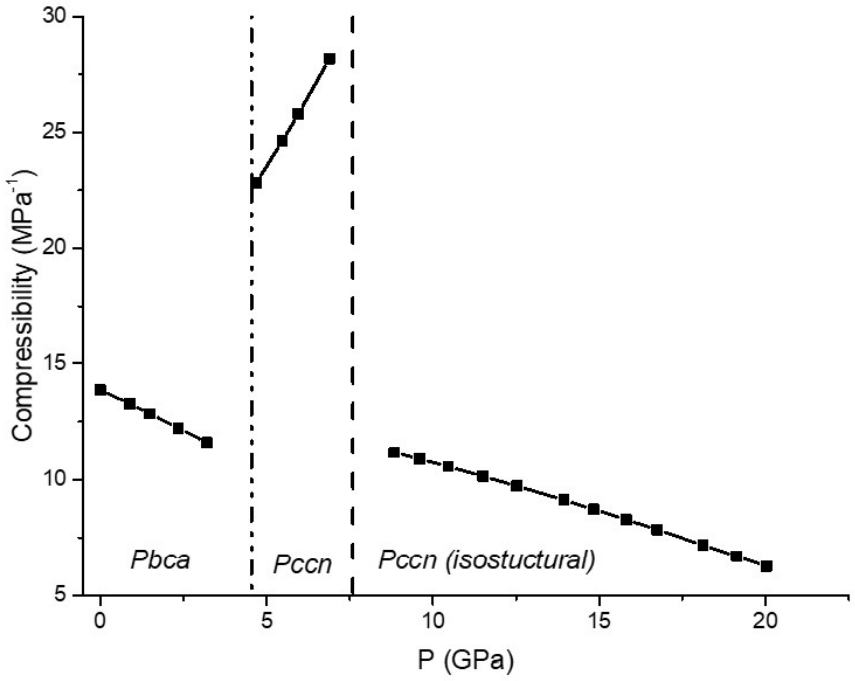

Figure 6. Isothermal compressibility κ_T vs. pressure from Eq. (2.14).

The Grüneisen parameter is used to correlate microscopic variation of materials with measurable macroscopic parameters in thermodynamics, as stated above. In order to correlate between pressure and mechanical, electronic structure in the studied HOIPs, the Grüneisen parameter as a function of pressure was calculated for 794 cm^{-1} ν_s(C-N), 931 cm^{-1}, 970 cm^{-1} and 1045 cm^{-1} β (C-H), 1212 cm^{-1} δ(C-H), 1496 cm^{-1} δ(NH_3^+) modes of $(PMA)_2PbI_4$ in the Pbca, Pccn, and Pccn(isostructural) phases at room temperature (Fig. 2). The parameter was observed to increase with increasing pressure for all the modes except for β (C-H) modes (Fig. 2). It is clear from Fig. 2 that there is a discontinuity in the Grüneisen parameter at 4.6 GPa and 7.7 GPa for all the modes. Although the crystal volume of $(PMA)_2PbI_4$ varied very slightly with pressure and the structural phase transition could not be seen explicitly at the volume data and Raman frequency data, substantial changes were observed between 0 and 20 GPa and an explicit discontinuity in the Grüneisen parameter at phase transition pressure (Fig. 2). Liu et al. too report a sharp rise in the band gap at 7.7 GPa, caused by inorganic layer structure distortion (Liu et al., 2018). The discontinuity in the Grüneisen parameter and the sharp rising in the band gap in $(PMA)_2PbI_4$ at 7.7 GPa was showed to be a isostructural phase transition due to the changes in the electronic structure of the studied HOIPs at this pressure. Tian et al. have inferred from high-pressure X-ray diffraction (XRD) measurements that a structural phase transition between Pbca and Pccn has occurred at 4.6 GPa (Tian et al., 2020), which was also detected in the Grüneisen parameter calculations in the present study. Although Tian et al. could determine no noticeable peak from the XRD measurements of $(PMA)_2PbI_4$ at 7.7 GPa, the Grüneisen parameter calculation in this research paper proved the occurrence of this phase transition.

The IR frequencies of the internal modes in HOIPs shifted slightly due to the pressure-induced variations in length and bend of atomic bond. In general, the bond length between atoms shrank, while the bending angle of Pb-I increased with the increasing pressure. Fig. 3 and 4 show that the wavenumbers (frequency) of β(C-H) and ν_s(C-N) modes in $(PMA)_2PbI_4$ tend to increase with pressure, and this behaviour is completely associated with the vibrations of organic ligand (PMA) in $(C_6H_5CH_2NH_3)_2PbI_4$. It is known that the distinctive internal IR modes in PMA, e.g., 784-1045 cm^{-1} β(C-H) bending mode in the benzene ring, 970-1212 cm^{-1}, ν_s(C-N) and δ(C-H) in the stretching mode, emerge at high frequencies (Cai, Lv, & Feng, 2012). The observed data and performed calculations too indicated this behavior. 1496 cm^{-1} IR mode (δ(NH_3) mode) corresponding to the N–H bending mode showed similar characteristic with β(C-H), ν_s(C-N) modes and exhibited blueshift as the pressure was increased. This behaviour can be ascribed to the enhancement of the inter-molecular interaction, specified the strengthening of pressure induced hydrogen bonds. $\nu_s(CH_2)$

Table 3

Values of the c_0 , c_1, and c_2 from Eq. (2.12)

$(PMA)_2PbI_4$	Pbca Phase		
$\nu_T(P)$	c_0 (cm^{-1})	c_1 (cm^{-1}/GPa)	c_2 (cm^{-1}/GPa^2)
784(cm^{-1}) ν_s(C-N)	-6.19 x10^{-3}	-5.64 x10^{-2}	-1.76 x10^{-1}
931(cm^{-1}) β(C-H)	-3.91 x10^{-2}	2.91 x10^{-1}	-9.59 x10^{-1}
970(cm^{-1}) β(C-H)	0	0	0
1045(cm^{-1})β(C-H)	9.20 x10^{-3}	-5.81 x10^{-2}	-2.00 x10^{-1}
1212(cm^{-1})δ(C-H)	-2.73 x10^{-2}	1.69 x10^{-1}	- 5.19 x10^{-1}
1496(cm^{-1})δ(NH_3^+)	1.36 x10^{-3}	-8.31 x10^{-3}	-5.91 x10^{-2}
2903(cm^{-1})ν_s(CH_2^+)	3.46 x10^{-2}	-2.81 x10^{-1}	9.25 x10^{-1}
3068(cm^{-1}) ν_s(NH_3^+)	-7.29 x10^{-3}	3.11 x10^{-2}	-1.43 x10^{-1}
	Pccn Phase		
784(cm^{-1}) ν_s(C-N)	2.27	-1.36	7.72 x10^{-3}
931(cm^{-1}) β(C-H)	7.48	-4.43	-8.29 x10^{-2}
970(cm^{-1}) β(C-H)	-9.77 x10^{-1}	6.32 x10^{-1}	6.26 x10^{-2}
1045(cm^{-1})β(C-H)	-4.59	2.81	9.06 x10^{-2}
1212(cm^{-1})δ(C-H)	9.83	-5.87	-1.50 x10^{-1}
1496(cm^{-1})δ(NH_3^+)	-5.44	3.37	1.05 x10^{-1}
2903(cm^{-1})ν_s(CH_2^+)	-7.48	4.48	-3.03
3068(cm^{-1}) ν_s(NH_3^+)	-6.78 x10^{-1}	3.96 x10^{-1}	-6.98 x10^{-3}
	Pccn(Isostructure) Phase		
784(cm^{-1}) ν_s(C-N)	-12.73	2.42	-1.34 x10^{-1}
931(cm^{-1}) β(C-H)	-	-	-
970(cm^{-1}) β(C-H)	-4.79	-3.20	2.86 x10^{-1}
1045(cm^{-1})β(C-H)	-54.93	10.24	-6.03 x10^{-1}
1212(cm^{-1})δ(C-H)	-9.25	1.80	-8.74 x10^{-2}
1496(cm^{-1})δ(NH_3^+)	14.77	-2.89	2.29 x10^{-1}
2903(cm^{-1})ν_s(CH_2^+)	36.75	-6.95	4.09 x10^{-1}
3068(cm^{-1}) ν_s(NH_3^+)	29.88	-5.61	3.39 x10^{-1}

(C-H stretching) and $\nu_s(NH_3)$ (N-H stretching) internal modes in $(PMA)_2PbI_4$ appeared at 2903 cm^{-1} and 3068 cm^{-1}, respectively (Fig. 5). These modes exhibited redshift unlike β(C-H), ν_s(C-N), and δ(C-H) modes with the increasing pressure. The reason for the redshift is that the electronegativity of a nitrogen atom is greater than that of a carbon atom. Due to this difference in charge, the distance between N and I atoms in $(PMA)_2PbI_4$ is shorter than the C-I atoms in the orthorhombic (Pbca) phase. Caused by these short bond lengths, the bond energy in the halide part of $(PMA)_2PbI_4$ reduces with the increasing pressure. As a result of the weakening in the bonding energy of the halide part, the IR frequency of $\nu_s(NH_3)$ and $\nu_s(CH_2)$ modes decrease owing to the increasing pressure, as observed experimentally and as evident in the calculations in Fig. 5. The mechanical and electronic structure of HOIPs and the order of molecules in $(PMA)_2PbI_4$ were slightly altered by the inducing pressure. It can be concluded that the shifts in the IR wavenumber of the modes in the studied HOIPs are directly related to these alterations.

Table 4

Bulk modulus value (intercept (K_0), slope (K_0')).

$(PMA)_2PbI_4$	K_0 (GPa)	K_0'	V_0 $(A^0)^3$	Pressure Interval (GPa)
Pbca	71.65	4.38	2291.61	0<P<4.6
Pccn	61.09	-3.72	2271.55	4.6<P<7.7
Pccn(Isostr.)	29.90	6.07	2085.83	7.7<P

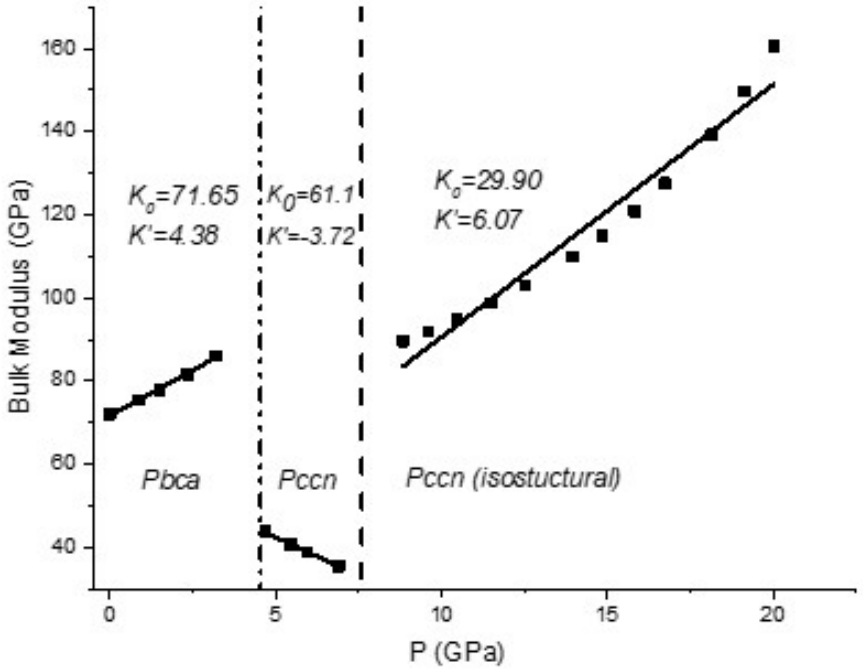

Figure 7. Isothermal Bulk modulus vs. pressure calculated from isothermal compressibility value (κ_T) for Pbca, Pccn, and Pccn(isostructural) phases of $(PMA)_2PbI_4$. Straight line corresponds to linear fit with coefficients (K_0) and (K_0') as in Table 4.

Isothermal compressibility coefficient of a solid is a measure of the relative volume change in response to a pressure change at a constant temperature. This parameter is very important in the fabrication of perovskite as is the case for all solid materials. The materials with large compressibility are desired in manufacturing processes because their crystal structure can be adjusted very effectively by compression. In this study, the pressure dependence of the isothermal compressibility for the orthorhombic-Pbca (0-4.6GPa), orthorhombic-Pccn (4.6-7.7 GPa), and orthorhombic-Pccn(isostructural) (7.7-20 GPa) phases were calculated through the Grüneisen parameter and the calculated IR frequency in $(PMA)_2PbI_4$ (Fig. 6). When pressure was increased, the compressibility ordinarily decreased for the Pbca and Pccn(isostructural) phases, but it abnormally increased for the Pccn phase. In addition, a sharp change in the compressibility was detected at 4.4 and 7.7 GPa in $(PMA)_2PbI_4$ (Fig. 6) due to the reordering of molecules in the vicinity of the phase transition pressure. The abnormal behaviour of $(PMA)_2PbI_4$ in the Pccn phase can be attributed to a weak van der Waals interaction between ligand (PMA^+) and metal halide framework. Crystals with a layered structure as in $(PMA)_2PbI_4$ mostly exhibit anisotropic behaviour under pressure owing to the various interactions between these layers (Tian et al., 2020). Another important parameter for fabrication processes of bulk materials is the bulk modulus, which refers to the inverse of the isothermal compressibility. Moreover, this parameter was calculated by using the calculated isothermal compressibility for all the phases in $(PMA)_2PbI_4$, as shown in Fig. 7 and Table 4. Tian et al. have determined the Bulk modulus value by fitting the third-order Brich-Murnaghan (BM) equation to the observed pressure-cell volume data (Tian et al., 2020). For the

Pbca phase (0-4.6 GPa), the current study's results ($K_0 = 71.65$ GPa, $K_0' = 4.38$) and Tian's findings ($K_0 = 73.57$ GPa, $K_0' = 4$) are almost the same. However, the results in this study are notably different from Titan et al's findings for the Pccn and Pccn(isostructural) phases (Table 4). The BM equation includes only the volume data, which are macroscopic parameters in thermodynamics (Birch, 1947), so the microscopic changes in the molecular structure cannot be analyzed explicitly. In the calculations, the microscopic changes through the Grüneisen parameter were taken into account, by which the isothermal compressibility and the bulk modulus were determined accurately.

4. Conclusion

In this study, the mechanical properties of $(PMA)_2PbI_4$, a good candidate for optoelectronic and photovoltaic applications, were analyzed in terms of pressure-induced phase transitions. The IR wavenumbers were calculated for the 794 cm^{-1} ν_s(C-N), 931 cm^{-1}, 970 cm^{-1} and 1045 cm^{-1} β (C-H), 1212 cm^{-1} δ(C-H), 1496 cm^{-1} δ(NH_3^+), 2903 cm^{-1} ν_s(CH_2^+), and 3068 cm^{-1} ν_s(NH_3^+) modes as the functions of pressure at room temperature in the Pbca, Pccn and Pccn(isostructural) phases of the $(PMA)_2PbI_4$ through the Grüneisen parameter. The calculated IR wavenumbers congruent with the observed data proved that the theoretical approach adopted for the purpose of this research study is practicable to calculate the pressure dependency of the IR wavenumber at room temperature. Besides, the isothermal compressibility and bulk modulus were calculated depending on pressure through the isothermal mode-Grüneisen parameter for the Pbca, Pccn and Pccn(isostructural) phases in $(PMA)_2PbI_4$. The results for the bulk modulus were in accord with those by Tian et al. (2020) only for the Pbca phase; however, the result for the Pccn and Pccn(isostructural) phases did not corroborate those of Tian et al.. One can adjust desirable mechanical and electronic properties of $(PMA)_2PbI_4$ by stretching or compressing in optoelectronic applications thanks to this small bulk modulus value.

Author Contributions

Arzu Kurt: Conceived and designed the analysis and wrote the paper.

Conflicts of Interest

The authors declare no conflict of interest.

References

Bandiello, E., Ávila, J., Gil-Escrig, L., Tekelenburg, E., Sessolo, M., & Bolink, H. J. (2016). Influence of mobile ions on the electroluminescence characteristics of methylammonium lead iodide perovskite diodes. Journal of Materials Chemistry A, 4(47), 18614-18620. doi: 10.1039/C6TA06854E

Birch, F. (1947). Finite Elastic Strain of Cubic Crystals. Physical Review, 71(11), 809-824. doi: 10.1103/PhysRev.71.809

Breternitz, J., & Schorr, S. (2018). What Defines a Perovskite? Advanced Energy Materials, 8(34), 1802366. doi: https://onlinelibrary.wiley.com/doi/10.1002/aenm.201802366

Cai, Y., Lv, J., & Feng, J. (2012). Spectral Characterization of Four Kinds of Biodegradable Plastics: Poly (Lactic Acid), Poly (Butylenes Adipate-Co-Terephthalate), Poly (Hydroxybutyrate-Co-Hydroxyvalerate) and Poly (Butylenes Succinate) with FTIR and Raman Spectroscopy. Journal of Polymers and the Environment, 21, 108-114. Doi: 10.1007/s10924-012-0534-2

Dou, L., Wong, A. B., Yu, Y., Lai, M., Kornienko, N., Eaton, S. W., . . . Yang, P. (2015). Atomically thin two-dimensional organic-inorganic hybrid perovskites. Science, 349(6255), 1518-1521. doi:10.1126/science.aac7660

Einstein, A. (1907). Die Plancksche Theorie der Strahlung und die Theorie der spezifischen Wärme. Annalen der Physik, 327(1), 180-190. doi: https://doi.org/10.1002/andp.19063270110

Fang, H.-H., Raissa, R., Abdu-Aguye, M., Adjokatse, S., Blake, G. R., Even, J., & Loi, M. A. (2015). Hybrid Perovskites: Photophysics of Organic–Inorganic Hybrid Lead Iodide Perovskite Single Crystals (Adv. Funct. Mater. 16/2015). Advanced Functional Materials, 25(16), 2346-2346. doi: https://doi.org/10.1002/adfm.201570107

Grüneisen, E. (1912). Theorie des festen Zustandes einatomiger Elemente. Annalen der Physik, 344(12), 257-306. doi: https://doi.org/10.1002/andp.19123441202

Kawano, N., Koshimizu, M., Sun, Y., Yahaba, N. F., Yutaka, Yanagida, T., & Asai, K. (2014). Effects of Organic Moieties on Luminescence Properties of Organic–Inorganic Layered Perovskite-Type Compounds. The Journal of Physical Chemistry C, 118(17), 9101-9106. doi: 10.1021/jp4114305

Kooijman, A., Muscarella, L. A., & Williams, R. M. (2019). Perovskite Thin Film Materials Stabilized and Enhanced by Zinc(II) Doping. Applied Sciences, 9(8), 1678. Doi: https://doi.org/10.3390/app9081678

Kurt, A. (2020). Pressure dependence of the Raman modes for orthorhombic and monoclinic phases of CsPbI3 at room temperature. Journal of Applied Physics, 128(7), 075106. doi: 10.1063/5.0012355

Liu, S., Li, F., Han, X., Xu, L., Yao, F., & Liu, Y. (2018). Preparation and Two-Photon Photoluminescence Properties of Organic Inorganic Hybrid Perovskites (C6H5CH2NH3)2PbBr4 and (C6H5CH2NH3)2PbI4. Applied Sciences, 8(11), 2286. Doi: https://doi.org/10.3390/app8112286

Mao, H.-K., Chen, X.-J., Ding, Y., Li, B., & Wang, L. (2018). Solids, liquids, and gases under high pressure. Reviews of Modern Physics, 90(1), 015007. doi: 10.1103/RevModPhys.90.015007

Ou, T., Liu, C., Yan, H., Han, Y., Wang, Q., Liu, X., . . . Gao, C. (2019). Effects of pressure on the ionic transport and photoelectrical properties of CsPbBr3. Applied Physics Letters, 114(6), 062105. doi: 10.1063/1.5079919

Ou, T., Ma, X., Yan, H., Shen, W., Liu, H., Han, Y., . . . Gao, C. (2018). Pressure effects on the inductive loop, mixed conduction, and photoresponsivity in formamidinium lead bromide perovskite. Applied Physics Letters, 113(26), 262105. doi: 10.1063/1.5063394

Planck, M. (1901). Ueber das Gesetz der Energieverteilung im Normalspectrum. Annalen der Physik, 309(3), 553-563. doi: https://doi.org/10.1002/andp.19013090310

Qin, X., Dong, H., & Hu, W. (2015). Green light-emitting diode from bromine based organic-inorganic halide perovskite. Science China Materials, 58(3), 186-191. doi: 10.1007/s40843-015-0035-4

Ren, X., Yan, X., Ahmad, A. S., Cheng, H., Li, Y., Zhao, Y., . . . Wang, S. (2019). Pressure-Induced Phase Transition and Band Gap Engineering in Propylammonium Lead Bromide Perovskite. The Journal of Physical Chemistry C, 123(24), 15204-15208. doi: 10.1021/acs.jpcc.9b02854

Ren, X., Yan, X., Gennep, D. V., Cheng, H., Wang, L., Li, Y., . . . Wang, S. (2020). Bandgap widening by pressure-induced disorder in two-dimensional lead halide perovskite. Applied Physics Letters, 116(10), 101901. doi: 10.1063/1.5143795

Stacey, F. D., & Hodgkinson, J. H. (2019). Thermodynamics with the Grüneisen parameter: Fundamentals and applications to high pressure physics and geophysics. Physics of the Earth and Planetary Interiors, 286, 42. doi: 10.1016/j.pepi.2018.10.006

Tian, C., Liang, Y., Chen, W., Huang, Y., Huang, X., Tian, F., & Yang, X. (2020). Hydrogen-bond enhancement triggered structural evolution and band gap engineering of hybrid perovskite (C6H5CH2NH3)2PbI4 under high pressure. Physical Chemistry Chemical Physics, 22(4), 1841-1846. doi: 10.1039/C9CP05904K

Wang, L., Ou, T., Wang, K., Xiao, G., Gao, C., & Zou, B. (2017). Pressure-induced structural evolution, optical and electronic transitions of nontoxic organometal halide perovskite-based methylammonium tin chloride. Applied Physics Letters, 111(23), 233901. doi: 10.1063/1.5004186

Wang, L., Wang, K., Xiao, G., Zeng, Q., & Zou, B. (2016). Pressure-Induced Structural Evolution and Band Gap Shifts of Organometal Halide Perovskite-Based Methylammonium Lead Chloride. The Journal of Physical Chemistry Letters, 7(24), 5273-5279. doi: 10.1021/acs.jpclett.6b02420

Wang, Y., Lü, X., Yang, W., Wen, T., Yang, L., Ren, X., . . . Zhao, Y. (2015). Pressure-Induced Phase Transformation, Reversible Amorphization, and Anomalous Visible Light Response in Organolead Bromide Perovskite. Journal of the American Chemical Society, 137(34), 11144-11149. doi: 10.1021/jacs.5b06346

Yang, S., Niu, W., Wang, A.-L., Fan, Z., Chen, B., Tan, C., . . . Zhang, H. (2017). Ultrathin Two-Dimensional Organic–Inorganic Hybrid Perovskite Nanosheets with Bright, Tunable Photoluminescence and High Stability. Angewandte Chemie International Edition, 56(15), 4252-4255. doi: https://doi.org/10.1002/anie.201701134

Yuan, Y., Liu, X.-F., Ma, X., Wang, X., Li, X., Xiao, J., . . . Wang, L. (2019). Large Band Gap Narrowing and Prolonged Carrier Lifetime of (C4H9NH3)2PbI4 under High Pressure. Advanced Science, 6(15), 1900240. doi: https://doi.org/10.1002/advs.201900240

Zhang, L., Wang, Y., Lv, J., & Ma, Y. (2017). Materials discovery at high pressures. Nature Reviews Materials, 2(4), 17005. doi: 10.1038/natrevmats.2017.5